Materials Advances

PAPER

View Article Online
View Journal

Cite this: DOI: 10.1039/d6ma00095a

Graphene-assisted porosity in acrylate-endcapped urethane-based hydrogels for biomedical applications

Josué M. Galindo, *[ab] Nicolas Deroose, [c] Beatriz García-Béjar, [d] Lana Van Damme,[c] María Arévalo-Villena, [d] Sonia Merino, [ab] Ester Vázquez, [ab] M. Antonia Herrero *[ab] and Peter Dubruel *[c]

Received 21st January 2026,
Accepted 27th March 2026

DOI: 10.1039/d6ma00095a

rsc.li/materials-advances

The development of advanced hybrid hydrogels is essential for biomedical applications, such as tissue engineering, drug delivery, and wound healing. The incorporation of additives, such as graphene, imparts specific functional properties to hydrogel networks. In this work, we report the successful integration of few-layer graphene (FLG) into acrylate-endcapped urethane (AUP) hydrogels, resulting in hybrid materials with enhanced structural and functional properties. Notably, the introducton of FLG induces the formation of a porous microstructure within an otherwise non-porous AUP network, representing a simple and effective strategy to generate porosity without the use of porogens or templating methods. This induced porosity is critical for promoting nutrient diffusion and cellular infiltration. In addition to this structural modification, FLG contributes to the reinforcement of hydrogels and influences the crystallization behavior, acting as a nucleating agent, highlighting its role as an active component in the hydrogel matrix rather than a passive filler. A comprehensive characterization, including mechanical, thermal, and morphological analyses, was conducted to elucidate the role of FLG within the hydrogel matrix. The resulting materials exhibit high gel fractions, tunable swelling behavior, and mechanical properties within the range relevant for soft tissue applications. *In vitro* cytotoxicity assays confirmed the biocompatibility of the FLG-enhanced hydrogels, validating their safety for potential biomedical applications. Antimicrobial assessment demonstrated a limited, concentration-dependent inhibition of bacterial growth, primarily at higher FLG contents. Overall, this study demonstrates a straightforward approach to engineer porous AUP-based hydrogels through FLG incorporation, expanding their potential for biomedical applications.

1. Introduction

The development of advanced hybrid hydrogels has gained significant attention in recent years, driven by their remarkable potential for a wide range of biomedical applications, including tissue engineering, drug delivery, and wound healing.[1–3] Hydrogels are 3D polymeric materials, assembled through a combination of physical interactions (involving hydrogen bonds, π–π stacking, van der Waals forces, and dipole–dipole interactions) and/or covalent bonds, that are able to absorb large amounts of water without dissolving in it.[4] Due to their three-dimensional and porous structure, together with the high water content, hydrogels impart exceptional properties, including flexibility, softness, and biocompatibility, rendering them exceptionally well-suited for diverse biological applications such as controlled drug delivery, tissue engineering, regenerative medicine, and biosensors.[5–11] Furthermore, the mentioned properties can be readily tailored by adjusting factors like the polymer content, the molar mass, and the crosslinking density.[12,13]

In this context, acrylate-endcapped urethane-containing polymers (AUP) are a class of polymers that have gained significant attention for the development of hydrogels. AUPs can be crosslinked, either in solid state or in solution, leading to hydrogels with varying water uptake capacities or other

---

[a] Faculty of Chemical Science and Technology, University of Castilla-La Mancha, Ciudad Real 13071, Spain. E-mail: Josue.MGalindo@uclm.es, MariaAntonia.Herrero@uclm.es
[b] Instituto Regional de Investigación Científica Aplicada (IRICA), University of Castilla-La Mancha, Ciudad Real 13071, Spain
[c] Polymer Chemistry & Biomaterials Group, Centre of Macromolecular Chemistry, Department of Organic and Macromolecular Chemistry, Ghent University, Krijgslaan 281 building S4, 9000 Ghent, Belgium. E-mail: Peter.Dubruel@UGent.be
[d] Department of Analytical Chemistry and Food Technology, University of Castilla-La Mancha, Ciudad Real 13071, Spain

physicochemical properties (*e.g.*, mechanical properties) which can be fine-tuned towards the intended application by carefully selecting their microstructure.[14–19] However, AUP-based hydrogels typically lack microporous structures, which is a critical limitation, particularly in biomedical applications. Unlike synthetic composites with homogeneous structures, biological composites evolve highly organised heterogeneous structures at multiple length scales, enabling them to achieve exceptional modulus, strength, and toughness simultaneously. Replicating the heterogeneous structures found in biological composites has been shown to be an effective strategy for developing high-performance, bioinspired structural composites.[20–23] Besides, porosity is a critical factor that can influence various aspects, since it plays a pivotal role in cell behaviour, the diffusion of nutrients, mass transport, and tissue formation.[24–28] Moreover, in the realm of wound healing, the porosity of hydrogels takes on a vital role by facilitating the retention of wound exudate, which is essential for creating a conducive, moist wound environment. Furthermore, the porous nature of these hydrogels would enable the exchange of gases, such as oxygen and carbon dioxide, between the wound and the external environment, which is crucial for promoting cell proliferation and tissue repair. Additionally, porosity further supports wound healing by facilitating the removal of metabolic waste while serving as a physical barrier against microbial infiltration, provided that the pore size is appropriately controlled.[15,29] Finally, the porous scaffolds offer the capability to encapsulate and precisely release drugs, growth factors, or other therapeutic agents at the wound site, enhancing their effectiveness in the healing process.[30]

Graphene and its derivatives have garnered significant attention as promising additives for the development of hybrid hydrogels, offering enhanced physicochemical and biological properties.[31] The distinctive capacity of graphene to engage in non-covalent interactions, such as π–π stacking, hydrogen bonding, and electrostatic forces, facilitates the binding of biomolecules, improving their bioavailability and stability. Upon incorporation into polymeric matrices, graphene can notably modify key mechanical properties,[32] including stiffness, porosity, and surface topography, factors that critically influence cellular behaviours such as adhesion, migration, and differentiation. Furthermore, graphene's exceptional electrical conductivity enables the electrical stimulation of cells, providing a novel means to regulate cellular functions. These hybrid materials can also be designed to respond to external stimuli, including electric and magnetic fields, thereby broadening their applicability in various biomedical contexts.[33–35]

In addition to their mechanical and electrical properties, graphene-based hydrogels exhibit outstanding thermal and chemical stability, making them suitable for applications in environments where exposure to extreme conditions is expected.[36,37] In wound healing, graphene has demonstrated considerable potential by stimulating the proliferation of key cell types, such as fibroblasts and keratinocytes, which are essential for tissue regeneration. Its ability to facilitate the controlled release of therapeutic agents further enhances the performance of drug delivery systems, promoting faster and more efficient healing. Additionally, the electrical conductivity of graphene supports electrical stimulation therapies, which have been shown to accelerate cell migration and tissue repair. Beyond these properties, graphene's potent antimicrobial activity offers an added benefit for wound care, helping to prevent infections in wound dressings.[38–41]

Hence, the synergistic combination of AUP-based hydrogels with graphene holds the potential to pave the way for the development of higher-performing hydrogels characterised by robust mechanical properties, particularly within the realm of biomedicine, with a notable focus on applications in wound healing.

Conventional AUP matrices are largely non-porous, limiting nutrient transport, cell infiltration, and overall biomedical performance. Here, we address this limitation by incorporating FLG into an AUP hydrogel for the first time, creating a porous and mechanically robust network that enhances diffusion, cell infiltration, and structural integrity.

A thorough characterization of the new hybrid materials was carried out, including gel fraction, swelling behaviour, photo-rheology, mechanical properties, Fourier transform infrared spectroscopy (FTIR), differential scanning calorimetry (DSC) and scanning electron microscopy (SEM) to better understand the influence of FLG within the hydrogel network, and the induction of pores. Besides, to verify the safety and biocompatibility of the developed materials, *in vitro* indirect cytotoxicity assays were performed. Finally, the antimicrobial properties of the hybrid hydrogels were assessed, highlighting the potentiality for wound healing applications.

2. Experimental part

2.1. Materials and reagents

Reagents were used as purchased from commercial sources without further purification. SP-1 graphite powder was purchased from Bay Carbon, Inc. and glycine from Acros organics (98%). Bisomer PEA6 (Geo Specialty Chemicals), butylated hydroxytoluene (BHT, Innochem GmbH), deuterated chloroform ($CDCl_3$, Euriso-Top), dimethyl terephthalate (DMT, Sigma-Aldrich), ethoxylated and propoxylated pentaerythritol triacrylate (EPPETA, Allnex), isophorone diisocyanate (IPDI, Sigma-Aldrich), phenothiazine (PTZ, Sigma-Aldrich), phosphoric acid (Sigma-Aldrich), triphenylphosphite (TPP, Honeywell Fluka), poly(ethylene glycol) 2000 g mol^{-1} (Sigma-Aldrich), Valikat bismuth neodecanoate catalyst (Umicore) were used as received. For the *in vitro* biological evaluation, Dulbecco's modified Eagle medium (DMEM, Sigma-Aldrich), maximum recovery diluent (MRD, Sigma-Aldrich), fetal bovine serum (FBS, Sigma-Aldrich), penicillin/streptomycin (P/S) (Sigma-Aldrich), calcein-acetoxymethyl/propidium iodide (Ca-AM/PI, Sigma-Aldrich), HFF (ATCC), 3-(4,5-dimethylthiazol-2-yl)-5-(3-carboxymethoxyphenyl)-2-(4-sulfophenyl)-2*H*-tetrazolium (MTS, Abcam), syringes (Filter service), ethanol (Chem-Lab), phosphate buffered saline (PBS) tablets (Sigma-Aldrich) were used as received. Tryptic soy broth (TSB), Mueller Hinton agar, yeast extract, peptone, glucose and bacteriological agar, which were used for preparing the culture medium, were supplied by Condalab (Spain). Sterile tubes and plates were purchased from Labbox Labware S.L while sterile 96-well plates and their sealing tape came from Thermo Fisher Scientific Inc. Yeast strains were obtained from the University of Castilla–La Mancha yeast culture collection (*Candida albicans* – UCLM 1632 and *Rhodotorula mucilaginosa* – UCLM 1662) while bacterial strains came from the Spanish Type Culture Collection (*Escherichia coli* – CECT515T and *Staphylococcus aureus* – CECT86T).

2.2. Synthesis of few-layer graphene (FLG)

FLG was prepared following a previous developed protocol.[42] In a standard procedure, 75 mg of graphite and 250 mg of glycine were subjected to ball milling (planetary ball mill Retsch pm100) in a 250 mL stainless steel jar, which contained 15 stainless steel balls (2 cm in diameter each). The milling was conducted at a speed of 100 rpm and at room temperature for 2 h. The resulting solid product was then dispersed and sonicated in 100 mL of water. This dispersion was subsequently transferred into a dialysis tubing (Spectrum labs, 3.5 kDa MWCO) and dialysed with water at room temperature, replacing the water every 2 hours, and continued overnight, in order to remove the glycine. Finally, the FLG aqueous dispersion was subjected to lyophilization, resulting in the production of FLG powder.

2.3. Synthesis of acrylate-endcapped urethane-based poly(ethyleneglycol) (AUP) precursors

The main components of the hydrogels, AUP-PEG2k (AUP-2k) di- and hex-acrylate, were synthesised following a protocol described by Pien *et al.*[43]

Prior to synthesis, the backbone (PEG with a molar mass of 2000 g mol^{-1}) was dried at 90 °C under vacuum (<30 mbar) with an Argon purge for 3 hours before the reaction. During this step, butylhydroxytoluene (BHT, 500 ppm) was added as an inhibitor, along with 164 ppm of phosphoric acid to neutralize the weak basicity of the PEG backbone, which was determined by titration with HCl. After complete drying, the temperature was lowered to 75 °C and IPDI (1 eq. relative to the amount of hydroxyl functionalities) was added, followed by bismuth neodecanoate (300 ppm) as catalyst. After 1 hour of reaction at 75 °C, the appropriate end-cap (Bisomer PEA6 or EPPETA for AUPPEG2 and AUPPEG6, respectively, 1 eq. relative to the amount of hydroxyl functionalities) was charged, followed by the same amount of catalyst as described before. The progress of the reaction was monitored by using FTIR spectroscopy, tracking the disappearance of the isocyanate stretching band at 2270 cm^{-1} (Fig. S1, SI). Also, ^1H NMR spectra were recorded to determine the acrylate content and confirm the chemical structure of the synthesised polymers (Fig. S2, SI). Finally, the resulting materials were poured on Teflon sheets to solidify and stored in the dark.

2.4. Synthesis of acrylate-endcapped urethane-based poly(ethyleneglycol)-FLG based hydrogels

Aqueous AUP (AUPPEG2 or AUPPEG6) solutions (30 wt%) were prepared using Milli-Q water as the solvent. To initiate the photopolymerization process, the photo-initiator LAP was added at a concentration of 2 mol% relative to the acrylate functionalities present in the AUP solutions. These AUP solutions were then used to create sheets by carefully pouring them between two glass plates covered with Teflon foil. The glass plates were separated by a spacer with a thickness of 1 mm. The final step involved irradiating the sheets with UV-A light (7.4 mW cm^{-2}) applied from both the top and bottom surfaces, with a curing time of 30 min.

In the case of hybrid materials incorporating few-layer graphene (FLG), different concentrations of FLG were introduced into the AUP solutions: 0.1 mg mL^{-1}, 0.25 mg mL^{-1}, and 0.5 mg mL^{-1}. For the 0.25 mg mL^{-1} and 0.5 mg mL^{-1} FLG concentrations, a heating process (60 °C, 30 min, stirring) was employed to ensure the uniform dispersion of FLG within both polymers.

LAP was synthesised following a previous described protocol.[44]

2.5. Characterization of FLG

Thermogravimetric analysis (TGA) was performed using a TGA Q50 (TA Instruments). The analysis started with a 20-minute isothermal step at 100 °C, followed by a temperature increase of 10 °C per minute up to 800 °C under a nitrogen atmosphere.

Raman spectra were obtained using a Renishaw inVia microspectrophotometer equipped with a 532 nm laser. The samples for Raman analysis were prepared by placing the powder onto double-sided tape.

Transmission electron microscopy (TEM) was conducted using a JEOL 2100 HRTEM system with an accelerating voltage of 200 kV. For TEM sample preparation, FLG was dispersed in ethanol (diluted) and sonicated for 2 minutes, then deposited on holey carbon grids (EMS). Images were captured using a Gatan Orius digital camera (2×2 MPi) under low-dose conditions (<5 mA).

Elemental analysis (EA) was performed in a LECO CHNS-932 analyzer (Model No. 601-800-500).

2.6. Characterization of AUP precursors and AUP hydrogels

The synthesised AUP material was characterised using proton nuclear magnetic resonance (^1H NMR) spectroscopy, performed on a Bruker Avance 300 MHz spectrometer at room temperature. The AUP was dissolved in deuterated chloroform ($CDCl_3$, Euriso-Top) to a concentration of 10 mg mL^{-1} prior to analysis. The acrylate concentration was determined using DMT as internal standard following previously published protocols.[43]

FTIR spectroscopy was performed using a PerkinElmer Frontier FTIR spectrometer, equipped with a MKII Golden Gate setup and a diamond crystal from Specac, operating in attenuated total reflection (ATR) mode. The IR spectra were recorded in the range of 600–4000 cm^{-1} with 6 scans, and the data were analysed using PerkinElmer Spectrum Analysis Software.

For gel fraction, the UV-cured hydrogel sheets were first cut into circular disks (ϕ = 12 mm, 1 mm thick). Subsequently, three samples of these disks were subjected to a freeze-drying process. The dry weight (w_d) was determined, followed by the incubation of the different samples in ultrapure water for 72 h at 20 °C. After the incubation period, the materials were once again subjected to freeze-drying, and the final dry weight (w_{fd}) was recorded. Gel fraction (G) was determined according to the following eqn (1).

$$G\ (\%) = \frac{w_{\mathrm{fd}}}{w_{\mathrm{d}}} \times 100 \tag{1}$$

In the case of swelling degree, also conducted in triplicate, the hydrogel disk samples (ϕ = 12 mm, 1 mm thick) were first immersed in Milli-Q water for 72 h at 20 °C to let any unreacted agents leach out effectively. Then, they were freeze-dried, and their initial dry weight (w_0) was determined. Subsequently, these dried samples were placed in Milli-Q water for an additional 72 hours to reach complete equilibrium. Afterwards, the weight of the swollen samples (w_s) was measured. To calculate the degree of swelling (S), eqn (2) was applied.

$$S = \frac{w_{\mathrm{s}} - w_0}{w_0} \tag{2}$$

For the *in situ* photo-rheology curing experiments, an Anton Paar Physica MCR 301 rheometer equipped with an Omnicure S1500 UV-A light source (λ = 320–390 nm) for sample irradiation from the bottom through a quartz plate was used. In this case, a parallel plate setup was used, using a top spindle with a diameter of 25 mm. In order to monitor the curing process, the storage moduli (G') and loss moduli (G'') of the aqueous AUP solutions (30 wt%; 2 mol% LAP; 300 μL) were recorded over time upon UV exposure (15 mW cm^{-2}) at 20 °C at a strain of 0.1% and a frequency of 1 Hz as these values were within the linear viscoelastic range of the polymers.[13] The gap between the two plates was initially set at 0.3 mm and the normal force was kept at 1 N after UV exposure. Storage and loss moduli of the materials were recorded before (3 min), during (30 min), and after (3 min) UV exposure after 45 min. Samples were recorded in triplicate.

Mechanical characterization was performed through tensile tests using a Tinius Olsen 5ST machine. The data was analysed using the Horizon Software. Dog bones (width: 4 mm, length: 50 mm, and thickness: 1 mm) were punched out of the UV-cured hydrogel samples, which were consequently incubated in ultrapure water for 72 h at 20 °C. After removal of excess water on the surface of the samples, the dimensions (width, length and thickness) of the swollen dog bones were again determined using a digital calliper. A 500 N load cell was used, in combination with a preload of 0.1 N and a speed of 10 mm min^{-1}. Next to the Young's modulus, the stress at break and elongation at break were determined.

The thermal properties of the AUP precursors were evaluated using differential scanning calorimetry (DSC) with a TA Instruments Q2000 DSC (Zellik, Belgium). Samples weighing 5–7 mg were placed in Tzero aluminum DSC pans, which were then sealed with aluminum Tzero lids. The samples were loaded into the furnace and equilibrated at 35 °C before starting the analysis. An initial heating cycle was performed to eliminate the samples' thermal history by heating them to 100 °C at a rate of 10 °C min^{-1}. The precursors were then cooled to −70 °C at a controlled rate of 10 °C min^{-1}. After this, the samples were reheated to 100 °C at a rate of 10 °C min^{-1}. The resulting DSC thermograms from the cooling and heating cycles were plotted against temperature.

Scanning electron microscope (SEM) analysis was carried out using a on a JCM-7000 benchtop SEM from JEOL. The samples were freeze-dried prior to attachment to the sample holder using double-sided carbon tape. They were subsequently sputter-coated (20 mA, 60 s, vacuum) with gold particles by an Automatic Au Sputter Coater EmiTech K550X with a RV3 two-stage rotary vane pump, resulting in a uniform layer of approximately 15–20 nm in thickness.

2.7. Cell test protocol

HFF were cultured in Dulbecco's modified Eagle medium (DMEM) with 10 v/v% FBS and 1 v/v% antibacterial penicillin/streptomycin (37 °C, 5% CO_2). Refreshment of the culture medium was performed every 2–3 days. Sub-culturing followed after reaching 80–90% confluency. HFF were used at passage number 12. In order to perform the different tests, disks (ϕ = 8 mm) were punched out of the synthesised hydrogel sheets. All samples were sterilised using UV-C irradiation (15 mW cm^{-2}) for 2 h. One sample was incubated per mL of culture medium during 1, 3, and 7 days. The effect of leachable components on the cell viability and metabolic activity was assessed in triplicate after 1, 3, and 7 days of leaching. To this end, 10 000 cells were seeded onto a 96 well-plate. Prior to evaluation, the cell medium was refreshed with 200 μL of the incubated medium and assessed after 24 h.

The metabolic activity was assessed through an MTS assay by preparing a mixture of 16 v/v% MTS in culture medium and subsequently adding it to the cells. After wrapping in tinfoil, the 96 well-plate was incubated in the dark (37 °C, 2 h) under continuous shaking. The MTS tetrazolium compound was bioreduced by viable cells into a brown-colored formazan product, which had an absorbance maximum at 490 nm. The absorbance at 490 nm was measured using an EL800 Universal Microplate Reader (BioTek Instruments) with the GEN5 software.

The live-dead viability assay was carried out by addition of a mixture of Ca-AM (0.2 v/v%) and PI (0.2 v/v%) in PBS to the cells, which were subsequently incubated in the dark (using aluminum foil) for 15 min at room temperature. Fluorescence microscopy was performed using an Olympus IX 81 with Xcellence Pro software together with a green fluorescent protein (GFP) filter and a Texas Red (TxRed) filter, which allowed for distinguishing living (green) from dead (red) cells.

2.8. Antimicrobial assessment procedure

Both antibacterial and antifungal activities were assessed in this study. *Staphylococcus aureus* (Gram-positive) and *Escherichia coli* (Gram-negative) were selected as representative bacterial strains for the antibacterial assay, while *Candida albicans* (Ascomycota) and *Rhodotorula mucilaginosa* (Basidiomycota) were chosen for the antifungal assay. The bacteria and yeast species were retrieved from −80 °C glycerol stocks, and 10 μL of each was inoculated into 5 mL of tryptic soy broth (TSB) and 5 mL of yeast extract peptone dextrose (YPD) broth (10 g L^{-1} yeast extract, 20 g L^{-1} glucose, 20 g L^{-1} peptone), respectively. For fresh cultures, bacteria were incubated at 37 °C for 24 hours without agitation, while yeasts were grown at 30 °C for 30 hours with gentle agitation (120 rpm). Overnight cultures were then used for both the serial dilution and disk diffusion methods.

Before antimicrobial testing, all AUPPEG2 and AUPPEG6 hydrogels were cut and standardised to a 0.4 cm diameter. The materials were sterilised under ultraviolet light for 1 hour before being used in both assays.

The protocol outlined by Ali *et al.*[45] was followed with slight modifications. Briefly, sterile AUPPEG2 and AUPPEG6 hydrogels were placed in triplicate on the bottom of 96-well plates. The cultures were adjusted to 10^6 cells mL^{-1} for bacteria by optical density at 600 nm or by using the Thoma cell counting chamber for yeast, with fresh TSB or YPD broth. Then, 200 μL of the cell suspensions were added to each well containing sterile hydrogels. Negative controls, containing only 200 μL of TSB or YPD broth without microorganisms, and growth controls, containing 200 μL of adjusted bacterial or fungal cultures without hydrogels, were also prepared in triplicate. The microplates were incubated at 37 °C for 24 hours (for bacteria) or 30 °C for 30 hours (for yeasts). Antimicrobial activity was evaluated by calculating the percentage of microbial growth reduction (eqn (3)). Colony-forming units (CFU) were counted at 0, 5, 10, and 24 hours for bacteria, and at 0, 7, 24, and 30 hours for yeast, using the drop plate method to obtain viable counts for each microorganism.[46]

$$\text{Microbial growth reduction percentage } (\%) = \left(\frac{\text{viable count of growth control} - \text{viable count of test}}{\text{viable count of growth control}}\right) \times 100 \tag{3}$$

Performance standards for antimicrobial disk susceptibility tests developed by CLSI (2012) was adapted for performing this analysis. Overnight bacterial and fungal cultures were grown as lawns on Mueller Hinton agar and YPD agar plates (10 g L^{-1} yeast extract, 20 g L^{-1} glucose, 20 g L^{-1} peptone, 20 g L^{-1} agar), respectively. Sterile hydrogel disks were then placed in duplicate on the surface of the cultured agar, and the system was incubated at 37 °C for 24 hours (for bacteria) or 30 °C for 48 hours (for yeasts). Based on the results from the "serial dilution method" section, the objective of this assay was to determine whether the AUP hydrogels inhibited or promoted the growth of microorganisms on the material.

In order to know if statistical differences existed, data collected from the quantitative analysis were subjected to an ANOVA test followed by a Duncan test using the IBM SPSS statistics v. 24.

3. Results and discussion

3.1. Preparation and characterization of FLG

FLG was synthesised using a previously established method that involves mechano-chemical exfoliation, with glycine serving as the exfoliating agent. The exfoliated FLG was suspended in water and subsequently dialysed to remove the glycine. The resulting aqueous FLG dispersion was then lyophilised to obtain a black powder.[42]

Thermogravimetric analysis (TGA) revealed a highly stable material, with a minimal weight loss of 3% at 600 °C, reflecting the presence of a low amount of functional groups in the FLG (Fig. 1A).[47] The Raman spectrum of FLG displayed characteristic peaks at 1346, 1580, 1621, and 2713 cm^{-1} corresponding to the D, G, D′, and 2D bands, respectively (Fig. 1B), providing structural insights. The G band, the most intense peak, corresponds to the sp^2-bonded carbon atoms in FLG. The D band indicates the presence of disorder in the FLG structure, which increases with the introduction of sp^3 hybridization. The ratio of the D and G bands (I_D/I_G), which quantifies the number of edge defects, was found to be 0.41, suggesting minimal defects.[48] The D′ band appears as a shoulder to the G band, and the 2D peak indicates that the FLG material consists of four layers (FWHM of 69.38 cm^{-1}), as determined by the method outlined by Paton *et al.*[49] The high-resolution transmission electron microscopy (HRTEM) analysis of FLG showed a lateral size distribution of 400 ± 26 nm (Fig. 1C and D). Finally, Fig. 1E presents the elemental analysis of FLG, revealing an oxygen percentage of 2.58 wt%, corroborating the observation from the

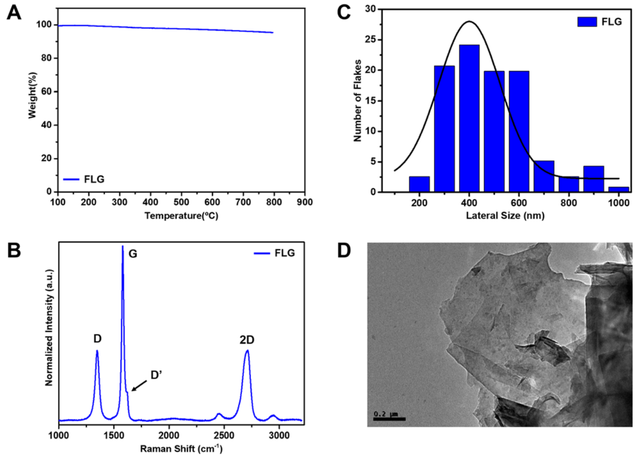

E

	%C	%H	%N	%S	%O
FLG	96.56 ± 0.33	0.33 ± 0.0	0.2 ± 0.01	0.33 ± 0.05	2.58 ± 0.08

Fig. 1 Characterisation of FLG material: (A) thermal stability analysis using TGA under nitrogen atmosphere, (B) chemical structure determination using Raman spectroscopy, (C) FLG size distribution using HRTEM, (D) representative FLG image using HRTEM and (E) FLG elemental analysis.

TGA analysis, in which the presence of a low amount of functional groups was noted.[47]

3.2. Synthesis of AUP-based hydrogels

AUP hydrogels were synthesised *via* radical polymerization of AUP-2k precursors. In this work, two types of hydrogels were developed using different AUP precursors of the same PEG backbone molar mass (2k): a diacrylate variant (AUPPEG2) and a hexa-acrylate variant (AUPPEG6) (Fig. 2A and B, respectively).

The synthesis of both precursors was performed as previously described in the literature.[43]

Hydrogels were prepared using the synthesised precursors following a previously established protocol.[15–17] For both hydrogel types (AUPPEG2 and AUPPEG6), a 30 wt% concentration of AUP precursors was selected, based on previous studies. Lithium 2,4,6-trimethylbenzoylphosphinate (LAP) was used as the photoinitiator at a concentration of 2 mol% relative to the acrylate content. LAP was chosen for its excellent reactivity under UV light, making it one of the most efficient photoinitiators, as well as for its high-water solubility and biocompatibility, key factors in the context of this research.[50–52] The mixture was stirred until achieving homogenization. Subsequently, the polymerization was performed at room temperature by irradiating with UV-A (λ = 320–390 nm) light for 30 min.

For the FLG-based AUP hydrogels, the same procedure was followed, while an AUP-FLG dispersion was used at FLG concentrations of 0.1, 0.25, and 0.5 mg mL^{-1}, allowing for the integration of FLG into the hydrogel matrices.

The structure and role of FLG in the hydrogel network were thoroughly characterised using different techniques.

3.3. Characterization of AUP-hybrid hydrogels

The incorporation of FLG into a 3D polymeric network has previously been reported by our group in various hydrogel systems, all synthesised through radical polymerization.[35,36,53,54] In these studies, FLG was introduced *in situ* during the synthesis process, resulting in a dispersion of FLG and all the monomers that constitute the hydrogel. It has been well-established that FLG was integrated into the network, becoming an active component of the structure and enhancing the properties of the resulting hydrogel. This was evidenced by a modification in both the swelling degree and pore size of the final hydrogel, suggesting that FLG plays a significant role within the network. Furthermore, the inclusion of FLG in the hydrogel matrix improved its mechanical properties, as indicated by increased Young's moduli.

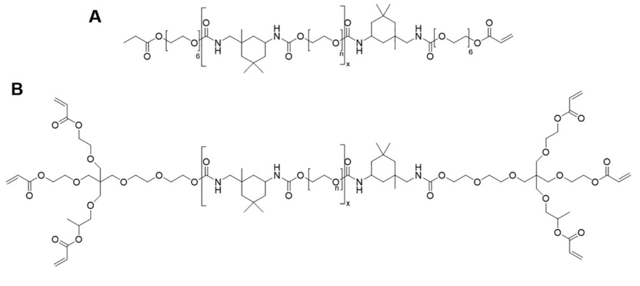

Fig. 2 Chemical structures of acrylate-endcapped, urethane-based poly(ethylene glycol) (AUP) precursors: diacrylated AUP (AUPPEG2) (A) and hexacrylated AUP (AUPEEG6) (B).

Additionally, the stability of the nanomaterial within the hydrogel network was assessed by Martin *et al.*, who introduced an FLG dispersion after polymerization and subjected the hydrogel to three cycles of swelling and deswelling in water. Notably, after three cycles, the FLG-based hydrogel, synthesised *via in situ* polymerization, maintained its structure, while the FLG absorbed post-synthesis was partially expelled. These findings suggested that FLG can serve as a covalent crosslinker in radical polymerization, likely due to the higher density of active double bonds on its surface. This feature opened the possibility for the development of novel hybrid hydrogels with enhanced properties based on FLG due to the ability of FLG to react covalently with ethylene-based monomers.[33]

Building on these previous studies, AUP hydrogels were thoroughly characterised to evaluate the potential effects of incorporating FLG into their network. For this, a range of analyses were performed, including gel fraction measurements, swelling tests, rheological studies, mechanical property assessments, Fourier transform infrared spectroscopy (FTIR), differential scanning calorimetry (DSC), and scanning electron microscopy (SEM).

The gel fraction (GF) of hydrogels holds significant importance, since it serves as a critical property, offering insights into the cross-linking efficiency of the polymeric materials. It refers to the proportion of a material that remains integrated within the network following equilibrium swelling in water, providing valuable information regarding whether the produced hydrogels require a purification step, such as leaching out the unreacted macromonomers, before their application. A high GF serves as an indicator of an efficiently crosslinked network. All gel fractions exceed 98% (Table 1, entry 1 and Fig. 3A). This observation suggests that FLG is successfully integrated into the network without disrupting or interfering with the crosslinking process. It further indicates that nearly all acrylate groups have reacted during crosslinking, ensuring the preservation of the network's integrity. As a result, stable, insoluble crosslinked networks are formed. These findings highlight the stability and structural integrity of the hydrogels, which are crucial characteristics for their potential biomedical applications.

The swelling degree provides valuable insights into the water-absorbing capacity of the hydrogels, which is vital for understanding their performance in various applications. It is influenced by several factors, including the volume fraction of the polymer, solvent interaction parameters, the molar mass between crosslinks, and the crosslinking density. Besides, alterations in the swelling ratio leads to differences in the mechanical properties of the network, as well as the diffusion rates of substances like ions, drugs, and nutrients through the hydrogel structure. For example, for biomedical or tissue engineering applications, swelling is exploited to mimic the extracellular matrix and to control the diffusion of bioactive molecules and cell migration into the network.[13] Large swelling

Table 1 Characterization of AUP hydrogels: gel fraction, swelling degree, storage modulus, Young's modulus, ultimate stress and ultimate elongation calculated from uniaxial tensile testing on swelled dogbone-shaped samples

		AUPPEG2				AUPPEG6			
Entry	Analysis	Blank	0.1 mg mL^{-1} FLG	0.25 mg mL^{-1} FLG	0.5 mg mL^{-1} FLG	Blank	0.1 mg mL^{-1} FLG	0.25 mg mL^{-1} FLG	0.5 mg mL^{-1} FLG
1	Gel fraction (%)	100.66 ± 0.58	98.91 ± 1.08	98.01 ± 2.28	99.06 ± 1.32	108.03 ± 3.79	98.85 ± 1.54	101.93 ± 3.60	100.54 ± 0.37
2	Swelling degree	3.82 ± 0.04	4.22 ± 0.08	4.18 ± 0.11	3.99 ± 0.01	2.78 ± 0.13	3.33 ± 0.16	2.78 ± 0.14	2.82 ± 0.05
3	Storage modulus (kPa)	99.15 ± 10.11	91.66 ± 4.69	88.96 ± 12.46	137.59 ± 18.56	140.87 ± 4.40	150.77 ± 2.57	150.87 ± 6.30	139.56 ± 19.02
4	Young's modulus (MPa)	0.65 ± 0.03	0.58 ± 0.04	0.62 ± 0.01	0.67 ± 0.02	1.18 ± 0.10	0.79 ± 0.04	1.00 ± 0.03	1.18 ± 0.06
5	Ultimate stress (MPa)	0.23 ± 0.05	0.19 ± 0.03	0.23 ± 0.05	0.20 ± 0.05	0.14 ± 0.02	0.12 ± 0.01	0.12 ± 0.02	0.15 ± 0.02
6	Ultimate elongation (MPa)	42.10 ± 5.92	41.47 ± 4.16	42.67 ± 10.80	41.60 ± 6.87	14.52 ± 0.79	16.76 ± 2.83	11.93 ± 1.85	17.70 ± 1.64

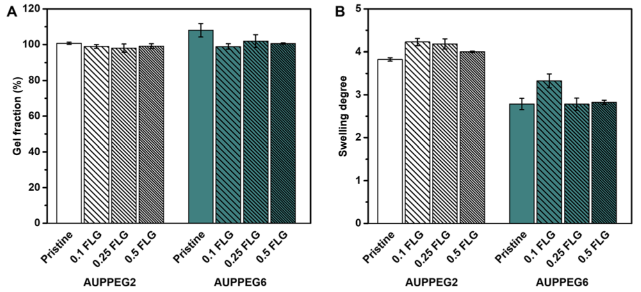

Fig. 3 (A) Gel fraction and (B) swelling degree of AUPPEG2 and AUPPEG6 pristine and hybrid hydrogels (*gel fractions higher that 100% are the result of experimental errors).

ratios may compromise the mechanical properties of hydrogels. Therefore, a balance between swelling ratio and mechanical properties has to be found.[55] Thus, the swelling ratio is a key parameter to consider in the biomedical field, as it affects the hydrogel's behavior and its interaction with biological environments.

As expected, increasing the acrylate content from 2 to 6 acrylates led to a significant reduction in the swelling ratio for both polymer backbones, attributable to the higher crosslinking density, consistent with previous studies.[43,56] However, after the introduction of FLG in the hydrogel network, a consistent trend was observed for both the diacrylate and the hexa-acrylate hydrogels: an initial slight increase in the swelling degree following the incorporation of FLG into the hydrogel network was noted, followed by a decrease in the swelling degree for higher FLG contents. This phenomenon can be attributed to the initial expansion of the hydrogel network upon introducing the FLG nanomaterial. However, as the FLG concentration, and thus the system's hydrophobicity increases, the network gradually swells less (Fig. 3B and Table 1, entry 2).

As mentioned, previous studies have shown that when FLG is incorporated into a hydrogel matrix *via in situ* polymerization, it becomes an integral part of the hydrogel network.[33–54]

To assess the impact of the AUP endcap and/or the introduction of FLG on the curing kinetics and the network formation of AUP hydrogels, *in situ* UV curing experiments using photo-rheology were conducted. The storage (G') and loss moduli (G'') of aqueous AUP solutions (30 wt%; 2 mol% LAP) before, during, and after UV-A irradiation were monitored. Fig. 4A and B display the curves obtained from the rheological tests for AUPPEG2 and AUPPEG6 hydrogels, respectively. Upon exposure to UV-A irradiation (after 50 seconds), the crosslinking reaction was initiated, resulting in a rapid and substantial increase in both moduli as the network formed swiftly. Results showed that there were no significant differences were observed between the pristine AUP hydrogels and their FLG-based counterparts, suggesting that FLG did not interfere with the kinetics of the polymerization process. Additionally, the storage moduli (G') of these samples were determined when hydrogel formation was complete (*cf.* G' values reach plateau) (Fig. 4C and Table 1, entry 3). In the case of AUPPEG2 hydrogels, a notable increase in the network G' was observed at the

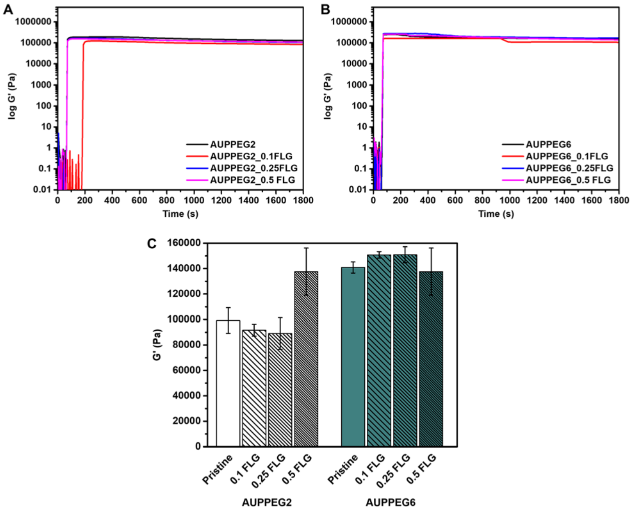

Fig. 4 Effect of FLG addition on UV crosslinking of AUPPEG as studied using photo-rheology. The data represent the evolution of G' for (A) AUPPEG2 and (B) AUPPEG6, while part (C) represents the obtained plateau values for the obtained G' values.

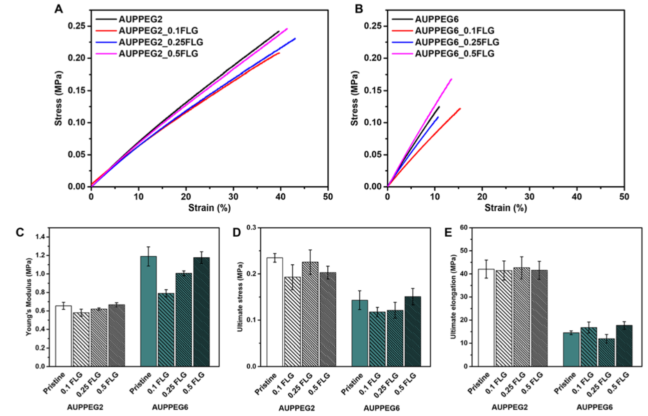

Fig. 5 Effect of FLG addition on the mechanical properties of AUPPEG hydrogels as studied using stress–strain tensile tests. (A) and (B) Represent the obtained curves for AUPPEG2 and AUPPEG6 hydrogels, respectively. (C) Young's modulus, (D) ultimate stress and (E) ultimate elongation of AUPPEG2 and AUPPEG6 hydrogels as derived from panels (A) and (B).

highest FLG concentration (0.5 mg mL^{-1} of FLG). This enhancement in the mechanical properties of the AUP hydrogel indicated that FLG reinforces the network.

Conversely, for AUPPEG6 hydrogels, an increase in the storage modulus as compared to AUPPEG2 was observed due to an increase in the crosslinking density. Regarding FLG-hybrid AUPPEG6 hydrogels, no significant differences were observed between the pristine hydrogels and the FLG-AUP counterparts. In this instance, the acrylate concentration relative to FLG is sufficiently high in the hexa-acrylated polymer that the incorporation of FLG has little to no effect on the mechanical properties of the gel.

To further investigate the mechanical properties of the synthesised AUPPEG2 and AUPPEG6 hydrogels, as well as the impact of FLG incorporation, tensile tests were conducted. The mechanical properties of hydrogels are crucial for their application in tissue engineering, as the structural integrity of the material is vital for supporting cell or tissue growth, with different tissues requiring specific mechanical characteristics.[57,58] Hydrogels are often designed to replicate the mechanical properties of the extracellular matrix (ECM) to create environments conducive to cellular behavior similar to *in vivo* conditions.

A commonly used parameter for assessing the mechanical properties of hydrogels is Young's modulus, which typically ranges from 0.1 kPa to 1 MPa, depending on the target tissue or organ type.[59,60] For optimal performance, a hydrogel scaffold should exhibit stiffness that closely matches the ECM, providing mechanical support for cell growth while maintaining its three-dimensional structure over time.[61]

Thus, the mechanical characteristics of the crosslinked AUP hydrogels were evaluated using tensile testing of dogbone-shaped samples. The obtained data allowed the determination of key parameters such as Young's modulus, ultimate stress, and ultimate elongation (Fig. 5 and Table 1, entries 4–6). A material that is more flexible exhibits easy deformation under low applied force, corresponding to a lower Young's modulus. In contrast, a stiffer material requires greater force for similar deformation, reflecting a higher Young's modulus. As anticipated, the hexa-acrylate-endcapped materials (AUPPEG6, both blank and FLG-hybrid) exhibited higher maximum stresses and Young's moduli compared to the di-acrylate-based materials (AUPPEG2, both blank and FLG-hybrid), which is consistent with the greater crosslinking density in the network. Considering the obtained Young's modulus values for these hydrogels (ranging from 0.6 to 1.2 MPa), they may also have potential applications in tissue engineering, particularly for cartilage or bone repair.[62]

FTIR analysis was performed to explore potential interactions between FLG and the AUP polymer network. Key absorption peaks were examined to verify the desired structure of the synthesised materials, particularly the N–H stretching (3300 cm^{-1}), C═O stretching (1720 cm^{-1}), and amide I and II bands (1530 and 1300 cm^{-1}, respectively). These peaks confirmed the formation of urethane linkages during the reaction between the alcohol groups (from the polymer backbone or endcap reagent) and the diisocyanate (IPDI). Additionally, the presence of acrylates was identified by the C═C stretch at 1640 cm^{-1} in the FTIR spectrum. However, due to the low concentration of FLG in the network, no significant differences were observed between the pristine materials and the FLG-hybrid variants (Fig. S3, SI).

Additionally, crystallinity is a critical concept in the field of polymer and materials science. It refers to the degree to which polymer chains in a material are arranged in an ordered, repeating, and three-dimensional pattern known as a crystal lattice. Polymers can exist in various states of crystallinity, and this property has a significant impact on their mechanical, thermal, and physical properties.[63] Nucleating agents are additives that promote the formation of smaller and more uniform crystals in polymers. These agents play a crucial role in controlling the crystallinity and, consequently, the properties of the final polymer product. The most potent nucleating agents typically possess high surface area and energy, low solubility in the polymer, efficient heterogeneous nucleation, compatibility with the polymer, high thermal stability and low concentration requirements.[64,65] In this sense, various studies have explored diverse nucleating agents, including carbon nanostructures.[66–68] Therefore, graphene could serve an efficient nucleating agent during the crystallization process, increasing both the degree and the speed of crystallization.[69,70] Moreover, as previously reported, graphene–polymer nanocomposites exhibit significantly enhanced mechanical properties.[71] Thus, to gain a comprehensive understanding of nucleation-driven crystallization, DSC was performed on both types of hydrogels and their FLG-hybrid counterparts (Fig. S4 and S5, SI). Notably, AUPPEG6 hydrogels did not exhibit crystallinity (Fig. S5, SI). In contrast, for AUPPEG2, exothermic crystallization peaks were observed between −20 and 20 °C (Fig. 6 and Fig. S4, SI). It is important to note that FLG acts as a nucleating agent, increasing the crystallization temperature (T_c) and enthalpy values (Table 2), as reported in the literature.[69]

Finally, the microstructures of the hybrid hydrogels AUPPEG2 and AUPPEG6 were analysed by scanning electron microscopy (SEM) (Fig. 7 and Fig. S6 and S7, SI). A noteworthy observation emerged from this analysis: following the incorporation of FLG into the hydrogel network, both hydrogels exhibited porosity in their microstructures. In the case of AUPPEG2 (Fig. 7A), the lower crosslinking density results in a less tightly interconnected network compared to AUPPEG6, where the presence of six acrylate groups leads to a more extensively crosslinked structure, rendering the pores less discernible (Fig. 7B). This behaviour can be attributed to the inherent hydrophobicity of FLG and its integration into the AUP hydrogel structure, which actively promotes pore formation within the hydrogel matrix. FLG plays a crucial role in the development of porosity within the material. It consists of hydrophobic nanosheets characterized by aromatic (ring-like) domains that tend to aggregate through π–π and hydrophobic interactions. However, the stacking of FLG sheets is hindered by the presence of AUP chains positioned between them in certain regions. This co-assembly drives the formation of microporous domains within the network. During photo-crosslinking, FLG undergoes radical coupling with the acrylate groups of AUP, further integrating FLG into the network and stabilizing the pores. Thus, upon UV irradiation, the AUP chains polymerize to form a crosslinked network in which FLG functions as an active structural component rather than a passive filler, stabilizing the porous architecture in the matrix.[72]

Table 2 Values of crystallization temperature (T_c), enthalpies (H) and melting temperatures (T_m) of AUPPEG2 and AUPPEG6 hydrogels

	AUPPEG2 hydrogel			AUPPEG6 hydrogel
	T_c (°C)	H (J g^{-1})	T_m (°C)	T_m (°C)
Blank	−2.31	43.34	32.13	25.44
+0.1 mg mL^{-1} FLG	5.12	48.13	31.75	25.73
+0.25 mg mL^{-1} FLG	2.18	49.25	33.35	25.25
+0.5 mg mL^{-1} FLG	2.38	45.26	31.76	25.11

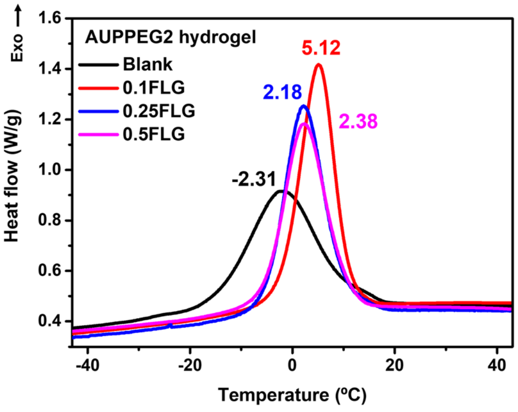

Fig. 6 DSC thermograms of AUPPEG2 and AUPPEG2-FLG hydrogels with T_c values.

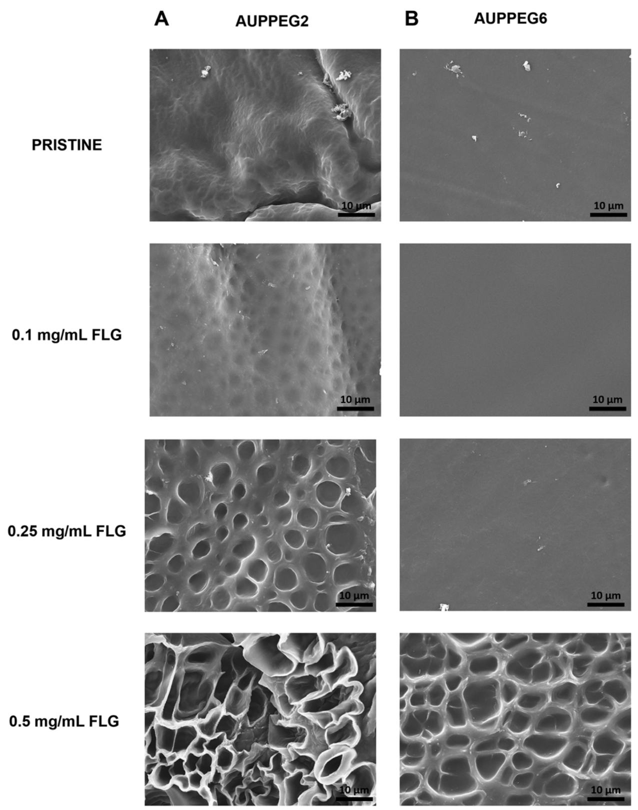

Fig. 7 Effect of FLG on the microstructure of (A) AUPPEG2 and (B) AUPPEG6 hydrogels, as studied using SEM.

As highlighted in the introduction, porous hydrogels have a broad range of applications across various fields, including catalysis, sensors, separation processes such as adsorption and membrane technologies, food science, agriculture, concrete additives, biomaterials, and drug delivery systems.[73–75] The presence of a porous microstructure significantly enhances the functionality of AUP hydrogels, enabling a wide array of advanced biomedical uses. The porous nature of these hydrogels after the incorporation of FLG allows for the controlled release of bioactive compounds, improved cell infiltration, and better integration with surrounding tissues, opening new doors for their application in regenerative medicine, implantable devices, and therapeutic systems. By optimising the porosity, AUP hydrogels have the potential to address complex challenges in tissue regeneration and personalised medicine, offering innovative solutions for a variety of medical conditions.

Therefore, the inclusion of FLG is crucial for the development of the porous structure in AUP-based hydrogels.

Subsequently, after establishing the influence of introducing FLG into the hydrogel matrix, it became essential to conduct cytotoxicity experiments to assess the potential harm these materials may pose. This evaluation is of utmost importance to ascertain their suitability for use in the biomedical field. Additionally, given the non-cytotoxic nature of both FLG and AUPs, it was essential to evaluate their combined biocompatibility, as well as to confirm that the inclusion of FLG into the network does not compromise the biological properties of the pristine network.

3.4. Indirect cell test

In order to assess the initial biocompatibility of the produced (FLG-containing) hydrogel materials, *in vitro* cell assays were performed. The assays performed were indirect tests, as the hydrogel matrix is PEG-based and therefore non-cell interactive. First, the 3-(4,5-dimethylthiazol-2-yl)-5-(3-carboxy-methoxyphenyl)-2-(4-sulfophenyl)-2*H*-tetrazolium (MTS) cell assay was performed in order to obtain information about the metabolic activity of the cells (Fig. 8A). Next, live/dead assay was performed to quantify the cell viability (Fig. 8B). The live/dead assay was combined with the MTS assay to enable a more comprehensive assessment of cell viability. While the MTS assay provides quantitative information on metabolic activity, it cannot distinguish whether high absorbance values result from increased cell numbers or elevated metabolic stress. The application of live/dead staining offers complementary qualitative insights into cell viability, density, and morphology, allowing for a more accurate interpretation of the MTS results. All cell tests were performed on human foreskin fibroblasts (HFF). All materials revealed cell viabilities over 92%, indicating that the incorporation of FLG into the hydrogel sheets did not affect the cell viability of the AUP. Furthermore, no significant differences ($p > 0.05$) were observed in terms of cell viability, except between the blank materials ($p < 0.05$). Overall, high metabolic activities of at least 80% were achieved, except for AUPPEG2 with 0.1 mg mL^{-1} of FLG.

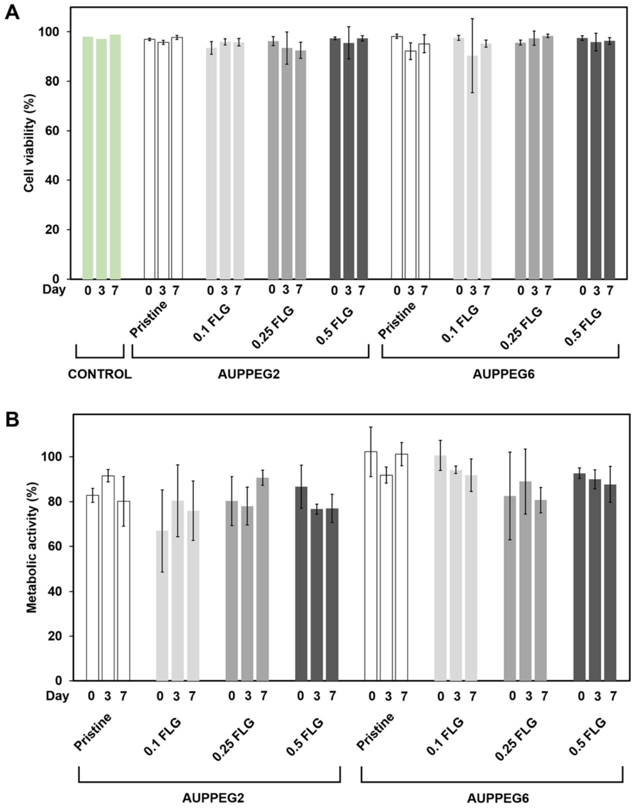

Fig. 8 Effect of FLG on the *in vitro* biocompatibility of AUPPEG2 and AUPPEG6 hydrogels, as studied by (A) the MTS indirect cell assay and (B) live/dead cell staining of both AUP blank and FLG-hybrid hydrogels.

3.5. Antimicrobial assessment

In an effort to understand the interactions between microorganisms and the herein developed AUP hydrogels, standardised laboratory methods were performed to determine the potential antibacterial and antifungal properties of these materials. Thus, bacteria (*Escherichia coli* and *Staphylococcus aureus*) and yeast (*Candida albicans* and *Rhodotorula mucilaginosa*) species were exposed to AUP hydrogels, both with and without FLG, to evaluate their antimicrobial properties. Initially, bacterial and yeast growth inhibition was assessed using a serial dilution method (Tables 3 and 4). In general, no reduction greater than 10% was observed for either bacteria or yeast at any of the sampling times, although a slight decreasing trend was noted. Additionally, *Rhodotorula mucilaginosa* showed significant resistance to the AUP-based hydrogels.

The AUPPEG2 pristine hydrogel did not interfere with the normal growth of bacteria throughout the entire monitoring period. The highest bacterial reductions were observed with AUPPEG2 containing 0.25 mg mL^{-1} FLG. For yeast species, the AUPPEG2 pristine hydrogel only impacted the growth of *Candida albicans*, with the most significant effect on growth occurring at 30 hours with AUPPEG2 containing 0.5 mg mL^{-1} FLG. In contrast, the growth of *Rhodotorula mucilaginosa* was affected only by AUPPEG2 with 0.25 mg mL^{-1} and 0.5 mg mL^{-1} FLG after at least 24 hours of exposure.

On the other hand, the AUPPEG6 pristine hydrogel slightly affected bacterial growth after 24 hours, with *Escherichia coli* showing the greatest reduction in cell count when exposed to 0.5 mg mL^{-1} FLG, while *Staphylococcus aureus* exhibited a higher reduction with 0.25 mg mL^{-1} FLG. For yeast species, similar levels of growth reduction were observed in *Candida albicans* at 30 hours, suggesting that the effect may be primarily due to the AUPPEG6 material itself. In contrast, the largest reduction in *Rhodotorula mucilaginosa* cell count occurred at

Table 3 Bacterial growth reduction percentage (mean ± SD) at 0 hours and after 5, 10 and 24 hours to hydrogels exposure (ni: no inhibition)

		Escherichia coli				*Staphylococcus aureus*			
AUPs hydrogels	FLG (mg mL^{-1})	0 h	5 h	10 h	24 h	0 h	5 h	10 h	24 h
AUPPEG2	Blank	ni	ni	ni	ni	ni	ni	ni	ni
	0.1	ni	ni	ni	3.96 ± 1.49	ni	1.34 ± 0.63	1.25 ± 0.36	6.46 ± 1.20
	0.25	ni	ni	ni	4.88 ± 1.16	ni	1.18 ± 0.39	1.63 ± 0.94	7.28 ± 1.76
	0.5	ni	0.69 ± 0.17	2.95 ± 0.31	2.06 ± 0.93	ni	0.67 ± 0.15	2.12 ± 0.21	5.01 ± 0.30
AUPPEG6	Blank	ni	ni	ni	3.58 ± 0.79	ni	ni	ni	2.21 ± 0.62
	0.1	ni	ni	ni	5.76 ± 1.28	ni	ni	1.04 ± 0.08	4.74 ± 0.27
	0.25	ni	ni	1.99 ± 0.42	5.45 ± 0.59	ni	0.97 ± 0.15	1.08 ± 0.14	4.05 ± 1.25
	0.5	ni	ni	5.56 ± 0.14	6.06 ± 2.46	ni	1.52 ± 0.15	2.85 ± 0.74	2.69 ± 0.82

Table 4 Fungal growth reduction percent (mean ± SD) at 0 hours and after 7, 24 and 30 hours to hydrogels exposure (ni: no inhibition)

		Candida albicans				*Rhodotorula mucilaginosa*			
AUPs hydrogels	FLG (mg mL^{-1})	0 h	7 h	24 h	30 h	0 h	7 h	24 h	30 h
AUPPEG2	Blank	ni	ni	ni	ni	ni	ni	ni	ni
	0.1	ni	1.95 ± 0.59	2.24 ± 0.52	3.64 ± 1.15	ni	ni	ni	ni
	0.25	ni	0.60 ± 0.15	2.23 ± 0.66	2.55 ± 1.08	ni	ni	ni	ni
	0.5	ni	1.06 ± 0.15	1.97 ± 0.20	1.99 ± 0.08	ni	ni	ni	3.53 ± 1.25
AUPPEG6	Blank	ni	1.47 ± 0.05	3.50 ± 0.19	4.37 ± 1.82	ni	ni	4.09 ± 1.46	6.64 ± 0.91
	0.1	ni	2.54 ± 1.12	4.48 ± 1.39	5.02 ± 0.57	ni	ni	ni	ni
	0.25	ni	3.39 ± 0.25	4.44 ± 1.03	5.57 ± 1.59	ni	ni	ni	6.52 ± 1.03
	0.5	ni	3.11 ± 0.16	3.84 ± 0.25	5.53 ± 1.89	ni	ni	2.93 ± 0.82	6.21 ± 1.55

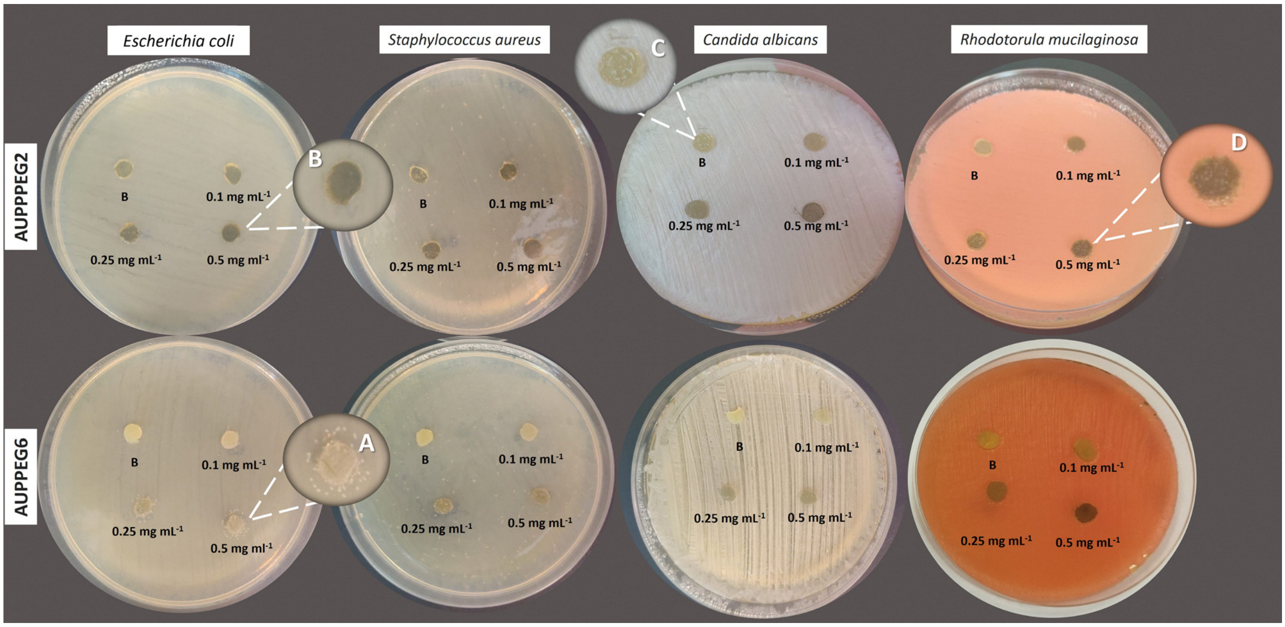

Fig. 9 Effect of FLG addition in AUPPEG hydrogels on bacterial growth as studied using the disk diffusion method. Examples of different types of growth: (A) partial halo inhibition, (B) no growth, (C) continuous growth, and (D) partial growth have been amplified for better visualisation.

30 hours, particularly against AUPPEG6 containing 0.1 mg mL^{-1} and 0.25 mg mL^{-1} FLG. However, statistical analysis indicated no significant differences between the samples, suggesting that the presence of FLG at various concentrations in the AUP-based materials does not substantially affect the growth of the surrounding microorganisms.

Building on these results, a disk diffusion method was employed to assess whether the studied microorganisms could grow on the AUP-based hydrogels or if these materials exhibited inert behaviour (Fig. 9). For the AUPPEG2 hydrogels, only the 0.5 mg mL^{-1} FLG concentration showed complete inhibition of bacterial growth after 24 hours of incubation (Fig. 9A). A similar effect was observed with *Staphylococcus aureus* when exposed to AUPPEG6 containing 0.5 mg mL^{-1} FLG, while *Escherichia coli* displayed a partial inhibition halo when exposed to AUPPEG6 at 0.25 and 0.5 mg mL^{-1} FLG (Fig. 9B). Regarding yeast species, *Candida albicans* was able to grow only on the pristine AUP-based hydrogels, whereas *Rhodotorula mucilaginosa* grew on all AUP-based hydrogels, regardless of FLG concentration (Fig. 9C).

Generally, the antimicrobial properties of other wound healing hydrogels have been linked to incorporated additives such as silver nanoparticles or antibiotics, rather than the inherent properties of the material itself.[76] In this case, the synthesised FLG-AUP hybrid hydrogels exhibited no signs of microbial growth, particularly bacteria, on their surface with specific FLG concentration, indicating a material that does not support the development of certain microorganisms under the tested conditions. This behavior may be attributed to the synergistic anti-adherent effects of graphene and the PEG component in the AUP polymer, but it could also be related to the interconnected porosity that hinders microbial infiltration.[15,77,78] Furthermore, the higher sensitivity observed in bacteria in the presence of this material is due to the fact that graphene demonstrates preferential interaction with bacterial membranes due to weaker intermolecular forces among bacterial phospholipids.[79] The application of AUPPEG2 and AUPPEG6 with 0.5 mg mL^{-1} FLG in wound healing could also be promising due to their favourable microbiological profile, in contrast to other graphene-based materials.[80] Since the interaction of AUP-based hydrogels with microorganisms is not yet fully understood, further investigation is needed, particularly to explore their dose-dependent activity and microbial specificity.

4. Conclusions

In this study, FLG was successfully incorporated into an AUP hydrogel matrix, using di- and hexa-acrylate-based AUP polymers. Optimization of the hydrogel material revealed that the integration of FLG did not interfere with the polymerization process. The resulting hybrid materials demonstrated significantly enhanced mechanical properties, particularly when 0.5 mg mL^{-1} of FLG was incorporated into the network. Furthermore, the incorporation of FLG induced porosity in the AUP hydrogels, a crucial feature for biomedical applications, as it facilitates nutrient and oxygen exchange and supports controlled drug release. Cytotoxicity assessments revealed that the hybrid materials maintained over 92% cell viability, indicating that FLG incorporation does not compromise the biocompatibility of the hydrogels. Finally, antimicrobial testing showed that the AUP-FLG hydrogels exhibited inert behaviour, preventing microbial growth, especially bacterial colonization, on their surfaces. These findings highlight the promising potential of FLG-incorporated AUP hydrogels for advanced biomedical applications, particularly in wound healing and other tissue-engineering applications.

Author contributions

Josué M. Galindo: investigation, writing – original draft, writing – review & editing, conceptualization. Nicolas Deroose: investigation. Beatriz-García Béjar: investigation, formal analysis, writing – original draft. Lana Van Damme: investigation. María Arévalo-Villena: writing – review & editing. Sonia Merino: writing – review & editing, supervision. Ester Vázquez: writing – review & editing, funding acquisition. M. Antonia Herrero: writing – review & editing, supervision, funding acquisition, conceptualization. Peter Dubruel: writing – review & editing, supervision, funding acquisition, conceptualization.

Conflicts of interest

There are no conflicts to declare.

Data availability

The data supporting this article have been included as part of the supplementary information (SI). Supplementary information is available. See DOI: https://doi.org/10.1039/d6ma00095a.

Acknowledgements

The authors are grateful for financial support from the Spanish Government (project PID2023-150894OB-I00), the Junta de Comunidades de Castilla-La Mancha (SBPLY/21/180501/000135/1) and University of Castilla-La Mancha (2022-GRIN-34076 Consolidado). This study forms part of the Advanced Materials programme and was supported by MCIN with funding from the European Union NextGenerationEU (PRTR-C17.I1) and the Junta de Comunidades de Castilla-La Mancha. J. M. Galindo acknowledges the Spanish Ministry of Economy and Competitiveness (MINECO) for his FPI Fellowship (FPI-PRE2018-084047) and the support of an international mobility grant from the Vice-Rectorate for Faculty and Professional Development, included within the Research Development Plan of the University of Castilla-La Mancha (BDNS (Identif.): 660787. [2022/10970]). N. Deroose would like to acknowledge the financial support of the Research Foundation Flanders (FWO) under the form of an FWO SB PhD fellowship (1S27323N). Finally, the authors would like to offer special thanks to the instrumentation team at the IRICA center for their valuable help with sample preparation and analysis.

References

1 M. M. Rana and H. De la Hoz Siegler, *Gels*, 2024, **10**(4), 216.
2 H. Chang, H. Wei, Y. Qi, S. Ding, H. Li and S. Si, *Cell Biol. Toxicol.*, 2025, **41**(1), 115.
3 H. Choi, W. S. Choi and J. O. Jeong, *Gels*, 2024, **10**(11), 693.
4 F. Ullah, M. B. H. Othman, F. Javed, Z. Ahmad and H. M. Akil, *Mater. Sci. Eng., C*, 2015, **57**, 414–433.
5 S. Merino, C. Martin, K. Kostarelos, M. Prato and E. Vazquez, *ACS Nano*, 2015, **9**(5), 4686–4697.

6 E. Caló and V. V. Khutoryanskiy, *Eur. Polym. J.*, 2015, **65**, 252–267.

7 K. Zöller, D. To and A. Bernkop-Schnürch, *Biomaterials*, 2025, **312**, 122718.

8 D. K. Patel, E. Jung, S. Priya, S.-Y. Won and S. S. Han, *Carbohydr. Polym.*, 2024, **323**, 121408.

9 Z.-C. Xu, Y.-Q. Yang, X.-W. Pang, Y.-T. Xu, L.-X. Gong, L.-C. Tang and S.-N. Li, *J. Mater. Sci. Technol.*, 2025, **237**, 10–19.

10 Y.-Q. Yang, X. Feng, X.-W. Pang, Y.-T. Xu, B. Jiang, Y. Xu, J. Wen, L.-X. Gong, L.-C. Tang, B. Wang and S.-N. Li, *J. Mater. Sci. Technol.*, 2026, **261**, 242–251.

11 Z.-F. Zeng, Y.-Q. Yang, X.-W. Pang, B. Jiang, L.-X. Gong, Z. Liu, L. Peng and S.-N. Li, *Adv. Funct. Mater.*, 2024, **34**(51), 2409855.

12 H. Yang, T. Liu, L. Jin, Y. Huang, X. Duan and H. Sun, *Nat. Commun.*, 2024, **15**(1), 9268.

13 J. Zhu and R. E. Marchant, *Expert Rev. Med. Devices*, 2011, **8**(5), 607–626.

14 M. Araújo, S. Van Vlierberghe, J. Feiteira, G.-J. Graulus, K. Van Tittelboom, J. C. Martins, P. Dubruel and N. De Belie, *Mater. Des.*, 2016, **98**, 215–222.

15 O. M. Ionescu, A. Mignon, M. Minsart, I.-D. Caruntu, S. E. Giusca, I. Gardikiotis, S. Van Vlierberghe and L. Profire, *Mater. Sci. Eng., C*, 2021, **130**, 112436.

16 M. Minsart, N. Deroose, L. Parmentier, S. Van Vlierberghe, A. Mignon and P. Dubruel, *Macromol. Biosci.*, 2023, **23**(3), e2200341.

17 A. Mignon, D. Pezzoli, E. Prouvé, L. Lévesque, A. Arslan, N. Pien, D. Schaubroeck, J. Van Hoorick, D. Mantovani and S. Van Vlierberghe, *React. Funct. Polym.*, 2019, **136**, 95–106.

18 M. Minsart, A. Mignon, A. Arslan, I. U. Allan, S. Van Vlierberghe and P. Dubruel, *Macromol. Mater. Eng.*, 2021, **306**(1), 2000529.

19 A. Houben, N. Pien, X. Lu, F. Bisi, J. Van Hoorick, M. N. Boone, P. Roose, H. Van den Bergen, D. Bontinck and T. Bowden, *Macromol. Biosci.*, 2016, **16**(12), 1883–1894.

20 Z. Tang, N. A. Kotov, S. Magonov and B. Ozturk, *Nat. Mater.*, 2003, **2**(6), 413–418.

21 R. Libanori, R. M. Erb, A. Reiser, H. Le Ferrand, M. J. Süess, R. Spolenak and A. R. Studart, *Nat. Commun.*, 2012, **3**(1), 1265.

22 P. Das, J.-M. Malho, K. Rahimi, F. H. Schacher, B. Wang, D. E. Demco and A. Walther, *Nat. Commun.*, 2015, **6**(1), 5967.

23 E. Munch, M. E. Launey, D. H. Alsem, E. Saiz, A. P. Tomsia and R. O. Ritchie, *Science*, 2008, **322**(5907), 1516–1520.

24 N. Annabi, J. W. Nichol, X. Zhong, C. Ji, S. Koshy, A. Khademhosseini and F. Dehghani, *Tissue Eng., Part B*, 2010, **16**(4), 371–383.

25 B. B. Mandal and S. C. Kundu, *Biomaterials*, 2009, **30**(15), 2956–2965.

26 A. Krsek, A. Jagodic and L. Baticic, *Medicina*, 2024, **60**(9), 1384.

27 W. Xue, D. Lee, Y. Kong, M. Kuss, Y. Huang, T. Kim, S. Chung, A. T. Dudley, S. H. Ro and B. Duan, *Adv. Funct. Mater.*, 2023, **33**(35), 2214129.

28 G. Lutzweiler, A. Ndreu Halili and N. Engin Vrana, *Pharmaceutics*, 2020, **12**(7), 602.

29 A. Shrivastav, A. K. Mishra, S. S. Ali, A. Ahmad, M. F. Abuzinadah and N. A. Khan, *Wound Med.*, 2018, **20**, 43–53.

30 I. Negut, G. Dorcioman and V. Grumezescu, *Polymers*, 2020, **12**(9), 2010.

31 G. Hong, S. Diao, A. L. Antaris and H. Dai, *Chem. Rev.*, 2015, **115**(9), 10816–10906.

32 H. P. Ferreira, D. Moura, A. T. Pereira, P. C. Henriques, C. C. Barrias, F. D. Magalhães and I. C. Gonçalves, *Int. J. Mol. Sci.*, 2022, **23**(4), 2312.

33 C. Martín, A. Martín-Pacheco, A. Naranjo, A. Criado, S. Merino, E. Díez-Barra, M. A. Herrero and E. Vázquez, *Nanoscale*, 2019, **11**(11), 4822–4830.

34 J. Leganés, A. M. Rodríguez, M. A. Arranz, C. A. Castillo-Sarmiento, I. Ballesteros-Yáñez, A. S. Migallón, S. Merino and E. Vázquez, *Mater. Today Chem.*, 2022, **23**, 100702.

35 J. Leganés Bayón, A. Sánchez-Migallón, Á. Díaz-Ortiz, C. A. Castillo, I. Ballesteros-Yáñez, S. Merino and E. Vázquez, *Chem. – Eur. J.*, 2020, **26**(71), 17069–17080.

36 C. Martín, S. Merino, J. M. González-Domínguez, R. Rauti, L. Ballerini, M. Prato and E. Vázquez, *Sci. Rep.*, 2017, **7**(1), 10942.

37 A. Servant, V. Leon, D. Jasim, L. Methven, P. Limousin, E. V. Fernandez-Pacheco, M. Prato and K. Kostarelos, *Adv. Healthcare Mater.*, 2014, **3**(8), 1334–1343.

38 A. Shariati, S. M. Hosseini, Z. Chegini, A. Seifalian and M. R. Arabestani, *Biomed. Pharmacother.*, 2023, **158**, 114184.

39 S. Saghazadeh, C. Rinoldi, M. Schot, S. S. Kashaf, F. Sharifi, E. Jalilian, K. Nuutila, G. Giatsidis, P. Mostafalu, H. Derakhshandeh, K. Yue, W. Swieszkowski, A. Memic, A. Tamayol and A. Khademhosseini, *Adv. Drug Delivery Rev.*, 2018, **127**, 138–166.

40 X. Ou, L. Guan, W. Guo, X. Zhang, S. Wu, D. Guo, R. Li, A. V. Zvyagin, Q. Lin and W. Qu, *Mater. Des.*, 2022, **224**, 111284.

41 G. Cao, J. Yan, X. Ning, Q. Zhang, Q. Wu, L. Bi, Y. Zhang, Y. Han and J. Guo, *Colloids Surf., B*, 2021, **200**, 111588.

42 V. J. González, A. M. Rodríguez, I. Payo and E. Vázquez, *Nanoscale Horiz.*, 2020, **5**(2), 331–335.

43 N. Pien, N. Deroose, M. Meeremans, C. Perneel, C.-Ş. Popovici, P. Dubruel, C. De Schauwer and S. Van Vlierberghe, *Biomater. Adv.*, 2024, **162**, 213923.

44 M. Markovic, J. Van Hoorick, K. Hölzl, M. Tromayer, P. Gruber, S. Nürnberger, P. Dubruel, S. Van Vlierberghe, R. Liska and A. Ovsianikov, *J. Nanotechnol. Eng. Med.*, 2015, **6**(2), 021001.

45 I. H. Ali, A. Ouf, F. Elshishiny, M. B. Taskin, J. Song, M. Dong, M. Chen, R. Siam and W. Mamdouh, *ACS Omega*, 2022, **7**(2), 1838–1850.

46 B. Herigstad, M. Hamilton and J. Heersink, *J. Microbiol. Methods*, 2001, **44**(2), 121–129.

47 J. M. González-Domínguez, V. León, M. I. Lucío, M. Prato and E. Vázquez, *Nat. Protoc.*, 2018, **13**, 495–506.

48 V. Yokaribas, S. Wagner, D. S. Schneider, P. Friebertshäuser, M. C. Lemme and C.-P. Fritzen, *Sensors*, 2017, **17**(12), 2937.

49 K. R. Paton, E. Varrla, C. Backes, R. J. Smith, U. Khan, A. O'Neill, C. Boland, M. Lotya, O. M. Istrate, P. King, T. Higgins, S. Barwich, P. May, P. Puczkarski, I. Ahmed, M. Moebius, H. Pettersson, E. Long, J. Coelho, S. E. O'Brien, E. K. McGuire, B. M. Sanchez, G. S. Duesberg, N. McEvoy, T. J. Pennycook, C. Downing, A. Crossley, V. Nicolosi and J. N. Coleman, *Nat. Mater.*, 2014, **13**(6), 624–630.

50 T. Majima, W. Schnabel and W. Weber, *Makromol. Chem.*, 1991, **192**(10), 2307–2315.

51 B. D. Fairbanks, M. P. Schwartz, C. N. Bowman and K. S. Anseth, *Biomaterials*, 2009, **30**(35), 6702–6707.

52 S. Benedikt, J. Wang, M. Markovic, N. Moszner, K. Dietliker, A. Ovsianikov, H. Grützmacher and R. Liska, *J. Polym. Sci., Part A:Polym. Chem.*, 2016, **54**(4), 473–479.

53 J. M. Galindo, C. M. Andreu, S. Merino, M. A. Herrero, E. Vázquez, A. M. Sánchez-Migallón and G. Castañeda, *Ecotoxicol. Environ. Saf.*, 2025, **292**, 117934.

54 J. M. Galindo, I. San-Millán, C. A. Castillo-Sarmiento, I. Ballesteros-Yáñez, M. A. Herrero, S. Merino and E. Vázquez, *Nanoscale*, 2023, **15**(34), 14238–14248.

55 F. Wu, Y. Pang and J. Liu, *Nat. Commun.*, 2020, **11**(1), 4502.

56 I. V. Khudyakov, *Prog. Org. Coat.*, 2018, **121**, 151–159.

57 G. Stojkov, Z. Niyazov, F. Picchioni and R. K. Bose, *Gels*, 2021, **7**(4), 255.

58 T. K. Meyvis, B. G. Stubbe, M. J. Van Steenbergen, W. E. Hennink, S. C. De Smedt and J. Demeester, *Int. J. Pharm.*, 2002, **244**(1–2), 163–168.

59 J. Liu, H. Zheng, P. S. P. Poh, H.-G. Machens and A. F. Schilling, *Int. J. Mol. Sci.*, 2015, **16**(7), 15997–16016.

60 M. S. B. Reddy, D. Ponnamma, R. Choudhary and K. K. Sadasivuni, *Polymers*, 2021, **13**(7), 1105.

61 H. Geckil, F. Xu, X. Zhang, S. Moon and U. Demirci, *Nanomedicine*, 2010, **5**(3), 469–484.

62 E. A. Kiyotake, M. E. Cheng, E. E. Thomas and M. S. Detamore, *Biomolecules*, 2022, **12**(6), 846.

63 Z. Zhang, Q. Li, C. Yesildag, C. Bartsch, X. Zhang, W. Liu, A. Loebus, Z. Su and M. C. Lensen, *Polymers*, 2018, **10**(9), 970.

64 G. Wypych, *Handbook of Nucleating Agents*, ChemTec Publishing, Toronto, 2016.

65 F. A. Wenzel, H. Welz, K. P. van der Zwan, S. Stäter, K. Kreger, R. Hildner, J. Senker and H.-W. Schmidt, *Macromolecules*, 2022, **55**(7), 2861–2871.

66 O. Agboola, E. R. Sadiku and T. Mokrani, *Design and Applications of Nanostructured Polymer Blends and Nanocomposite Systems*, William Andrew Publishing, Boston, 2016.

67 Z. Liu, K. Chen and D. Yan, *Eur. Polym. J.*, 2003, **39**(12), 2359–2366.

68 Q. Yuan, S. Awate and R. Misra, *Eur. Polym. J.*, 2006, **42**(9), 1994–2003.

69 H. C. Bidsorkhi, A. G. D'Aloia, G. De Bellis, A. Proietti, A. Rinaldi, M. Fortunato, P. Ballirano, M. P. Bracciale, M. L. Santarelli and M. S. Sarto, *Mater. Today Commun.*, 2017, **11**, 163–173.

70 R. Zhang, K. Jariyavidyanont, B. Wang, E. Zhuravlev, X. He, C. Schick and R. Androsch, *Polymer*, 2025, **335**, 128813.

71 S. Lee, J.-Y. Hong and J. Jang, *Polym. Int.*, 2013, **62**(6), 901–908.

72 C. Teng, J. Qiao, J. Wang, L. Jiang and Y. Zhu, *ACS Nano*, 2016, **10**(1), 413–420.

73 R. Foudazi, R. Zowada, I. Manas-Zloczower and D. L. Feke, *Langmuir*, 2023, **39**(6), 2092–2111.

74 L. A. Sharpe, A. M. Daily, S. D. Horava and N. A. Peppas, *Expert Opin. Drug Delivery*, 2014, **11**(6), 901–915.

75 X. Sun, F. Yao and J. Li, *J. Mater. Chem. A*, 2020, **8**(36), 18605–18623.

76 J. Delaey, P. Dubruel and S. Van Vlierberghe, *Adv. Funct. Mater.*, 2020, **30**(44), 1909047.

77 M.-Y. Xia, Y. Xie, C.-H. Yu, G.-Y. Chen, Y.-H. Li, T. Zhang and Q. Peng, *J. Controlled Release*, 2019, **307**, 16–31.

78 M. Abrigo, P. Kingshott and S. L. McArthur, *Biointerphases*, 2015, **10**(4), 301.

79 V. Lanai, Y. Chen, E. Naumovska, S. Pandit, E. Schröder, I. Mijakovic and S. Rahimi, *Nanoscale*, 2024, **16**(3), 1156–1166.

80 S. P. Couvillion, R. E. Danczak, X. Cao, Q. Yang, T. P. Keerthisinghe, R. S. McClure, D. Bitounis, M. C. Burnet, S. J. Fansler, R. E. Richardson, M. Fang, W.-J. Qian, P. Demokritou and B. D. Thrall, *NanoImpact*, 2023, **30**, 100463.